Highlights

Use of truncated Fisher sensitivity analysis for design verification of mechanical systems under uncertainty

Jiannan Yang, Jerome Jarrett

- A new data driven sensitivity method to reduce simulation and measurement discrepancy
- Fisher information based regional sensitivity analysis that captures complex parameter interactions
- One-sample approach where sensitivity analysis comes at no additional cost to uncertainty analysis

Use of truncated Fisher sensitivity analysis for design verification of mechanical systems under uncertainty

Jiannan Yang[a,*], Jerome Jarrett[b]

[a]*School of Physics, Engineering and Technology, University of York, Heslington, York, YO10 5DD, UK*
[b]*Department of Engineering, University of Cambridge, Trumpington Street, Cambridge, CB2 1PZ, UK*

Abstract

Sensitivity analysis is becoming an essential part of simulation based engineering design, but few sensitivity methods can directly consider measurement data for design verification. Here we present a new data-driven method, based on the truncated Fisher Information Matrix (tFIM), to identify the key drivers of the discrepancy between simulated and measured frequency response function and to guide the design verification process. We found tFIM is as effective as the more commonly used Monte Carlo Filtering (MCF) for design verification, but offers additional insights to sensitivity information from parameter interactions and from within the truncated region. To overcome the non-desirable issue of a fixed truncation, we discuss the augmentation of the input parameters by random truncation thresholds. Application of tFIM to the dynamics verification of a model floating wind turbine successfully identifies the most important parameter out of 15 input random variables, and the sensitivity guided design update is parsimonious and interpretable. Thanks to its efficiency as a one-sample approach, we expect the new tFIM method to complement global uncertainty and sensitivity analysis and become an integral part of design verification for the dynamic performance of mechanical systems under uncertainties.

Keywords: regional sensitivity analysis, frequency response, model updating, wave tank testing, offshore wind turbine

1. Introduction

This research is motivated by applications of global sensitivity analysis (GSA) towards design, development and verification of mechanical systems. The importance of sensitivity analysis for simulation based engineering design has long been recognized, particularly in the presence of uncertainties. The input data for the simulation models are often uncertain as they could be from multiple sources and of different levels of relevance. The uncertain inputs induce output uncertainties in the design quantities of interest. Sensitivity analysis

*Corresponding author
Email address: `jiannan.yang@york.ac.uk` (Jiannan Yang)

can examine the input-output relationship and identify the influential inputs, thus becoming an integral part of the engineering design process.

A widely applied category of GSA is the variance-based approach [1]. Variance-based methods, also called Sobol' indices, decompose the function output into a linear combination of input and interaction of increasing dimensionality, and estimate the contribution of each input factor to the variance of the output [2]. However, the estimation of Sobol' indices can become expensive in terms of the number of model evaluations. For example, the computational cost using sampling based estimation for variance-based indices is $N(d+1)$ [2], where N is the base sample number and d is the input dimension. Large values of N, normally in the order of thousands or tenths of thousands, are needed for more accurate estimate, and the computational cost has been noted as one of the main drawbacks of variance-based sensitivity indices [2].

To mitigate the computational issues, for engineering problems, surrogate models such as polynomial and Kriging models are often employed. Efficient analytical techniques based on metamodels have been developed for variance-based sensitivity analysis of simulation based design [3]. A variant of the variance based methods, called distributional sensitivity analysis, has been applied to simulation based design [4]. This method regards the amount of variance reduction of inputs as random variables, which relaxes the assumption of conventional variance-based methods that the uncertainty can be completely reduced as that assumption is rarely possible in engineering design.

Despite its wide application, the variance-based methods are inherently limited to the second moment of the model output. This limitation can be overcome by examining the sensitivity of the probability density function (PDF) of the model outputs.

This approach has been studied for engineering design using the divergence between two PDFs corresponding to before and after uncertainty reduction of the random variable of interest [5]. This utilizes the concept of omission sensitivity, where a random variable is made deterministic to eliminate its uncertainty. Different from [5], the design tailored sensitivity metric [6] utilises the Fisher Information Matrix (FIM) to examine the impact on the joint PDFs of the design outputs, from a simultaneous variation of the input uncertain variables. Other distance measures have also been used for sensitivity analysis, including the mutual information [7], relative entropy and the Hellinger distance [8]. A review of distribution-based sensitivity methods can be found in [9].

Much of the aforementioned work has focused on developing sensitivity metrics for the global design space. To link the design space and the design requirements, Monte Carlo Filtering (MCF) is commonly used. For example, MCF-based sensitivity analysis has been applied to the design verification of nuclear turbosets [10], where the specific verification criteria can be taken into account. In the process design of chemical engineering [11], Sobol' method is first used to eliminate non-influential input variables, and with reduced dimension, MCF is then used for determining and adjusting critical variables to achieve acceptable performance of the output. In building design [12], the Morris method [13] is first used to screen insignificant design inputs at the early building design stage to assess energy demand, thermal comfort, and daylight, and MCF is then used to link the design space to the requirements and design choices.

MCF is widely applied due to its easy implementation, where only a single set of Monte Carlo samples is required (one-sample approach), and its straightforward filtering interpretation to target verification requirements. However, compared with many global sensitivity analysis methods, MCF is not effective at revealing complex structures of parameter interactions and the contribution from products of parameters that might compensate.

Inspired by the effectiveness of filtering to target a specific design region of interest, in this paper, we present a new regional sensitivity analysis method for design verification. The key idea here is to combine the Fisher information with the truncated probability distribution that is conditional on the measured verification data. The newly formed truncated Fisher Information Matrix (tFIM) is shown to identify the key drivers of the discrepancy between simulation and measurement in the presence of uncertainties. tFIM performs similarly to MCF, but is more effective for complex parameter interaction structures and provides additional insights to sensitivity information within the truncated region. And that is the main contribution of this paper.

To overcome the non-desirable issue of truncation or filtering with fixed bounds, we discuss the augmentation of the input parameters by random truncation thresholds. Application of tFIM to the design verification of a model floating wind turbine demonstrates that the key drivers of discrepancy tend to have strong interactions with the random thresholds, and that provides a more robust strategy as no arbitrary fixed bound is assumed for the truncation.

We note that the truncated probability distribution measures the degree of misfit between the measured data and simulations and plays the role of approximating the likelihood function. Sensitivity analysis using tFIM thus adopts similar principle as the GSA-GLUE approach [14], where GSA is applied to the likelihood measure so that the sensitivity analysis is conditioned on observed data. However, unlike GSA-GLUE which uses generalised likelihood values [15], tFIM makes no assumption of the form of the likelihood function. tFIM instead makes approximations using a distance function via simulations, similar to rejection based Approximate Bayesian Computation (ABC) methods (see e.g. ABC tutorial [16]). In addition, GSA-GLUE is based on Sobol' indices, while tFIM utilises Fisher information that is not limited to the second moment and is applicable for a more diverse type of data distribution.

Note that sensitivity analysis have often been used to select a subset of parameters for the purpose of model updating. tFIM proposed in this paper can be used similarly to identify parameter subsets for model updating in a lower dimensional parameter space. Different from many local [17] or global SA [18] methods used for model updating with a Gaussian error assumption, however, tFIM utilises regional SA methods with ABC type of truncations to take into account multiple sources of uncertainty in the design verification process. More importantly, tFIM examines the parameter interactions between the truncation and model parameters, thus helping the designers and engineers with an improved understanding for the causes of the discrepancy.

In what follows, we first define the design verification problem for the dynamic performance of a mechanical system and explain the research motivation in Section 2. A new data driven approach using truncated Fisher information is introduced in Section 3. In Section 4, we conduct numerical benchmarks to validate the proposed method. In Section 5, the application of sensitivity analysis to guide the design verification is presented in detail using a case study of model floating wind turbine design. And concluding remarks are given in Section 6.

2. Problem setting and motivation

2.1. Problem setting

Modelling and simulation is playing an ever growing role in the process of design verification, to ensure the mechanical design meets its specifications and intended purpose. This research aims to utilise sensitivity analysis to guide designers and engineers towards design, development and verification of mechanical systems.

In this paper, we focus on the design verification for the dynamic performance of a mechanical system. In this setting, the behaviour of a mechanical system, at a particular frequency ω, is most commonly described by its frequency response as:

$$\boldsymbol{\phi}(\omega, \mathbf{x}) = \mathbf{H}(\omega, \mathbf{x})\mathbf{f}(\omega) \tag{1}$$

where $\mathbf{x}$ is the design parameter vector that we use to describe the system of interest and $\mathbf{f}(\omega)$ is the excitation vector at frequency ω.

$\mathbf{H} \in \mathbb{C}^{\mu\times\mu}$ is the frequency response function (FRF) matrix, which for a linear system can be found as the inverse of the dynamic stiffness matrix:

$$\mathbf{H}(\omega, \mathbf{x}) = \left[-\omega^2\mathbf{M}(\mathbf{x}) + i\omega\mathbf{C}(\mathbf{x}) + \mathbf{K}(\mathbf{x})\right]^{-1} \tag{2}$$

where $\mathbf{M}(\mathbf{x})$ is the mass matrix, $\mathbf{C}(\mathbf{x})$ is the damping matrix, and $\mathbf{K}(\mathbf{x})$ is the stiffness matrix.

During design verification, one of the main objectives is to reduce the discrepancy $\mathbf{y_d}$ between our model simulation and the measurement:

$$\mathbf{y_d}(\omega, \mathbf{x}) = \boldsymbol{\phi}(\omega, \mathbf{x}) - \boldsymbol{\phi}_m(\omega) \tag{3}$$

where the subscript m indicates measured outputs.

A typical approach at this stage is to adjust the parameters in the computational model, using methods such as model updating [19], to improve agreement with the measured data. In the presence of uncertainties, not only the nominal values, but also the statistical variabilities of the design parameters need to be considered. A drawback of this approach for design verification is that there is little insight into the root causes of the discrepancy.

2.2. Motivation for sensitivity guided verification

As an alternative to adjusting the entire set of parameters to reduce the discrepancies, a subset of parameters can be targeted to update our numerical model [17]. In the presence of uncertainties, GSA methods can be used. For example, for model updating, a composite Sobol' sensitivity index has been proposed to discriminate parameters with correctly modelled statistics from the erroneous ones under Gaussian noise assumption [18]. The identified parameter subsets can then be used improve the model simulation in a lower dimensional parameter space.

More importantly for design verification, GSA can help the designers and engineers with an improved understanding for the causes of the discrepancy. For example, in the case study described in Section 5, a mismatch between the proposed design and the physical set up has been successfully identified as the key driver for the simulation measurement discrepancy, thanks to a sensitivity guided analysis.

However, most of the existing GSA methods cannot be used directly to target the discrepancy reduction, because they are based purely on simulated data.

For example, it is clear from Eq.3 that $\frac{\partial y_d}{\partial x} = \frac{\partial \phi}{\partial x}$, since $\phi_m(\omega)$ is not a function of the model parameters, i.e. a constant with respect to variations of x. In addition, as the variance of an uncertain variable is translation invariant, i.e. $Var(y_d) = Var(\phi)$, there is no effect of the measured data ϕ_m in the estimation of the Sobol' sensitivity indices.

Regionalised sensitivity analysis (RSA), on the other hand, examines which input parameter is most important for a specified region of the output [2]. RSA is thus well positioned to link the design space and the design requirements for design verification, and the most intuitive and widely used method is the Monte Carlo Filtering (MCF) method as discussed in the introduction.

In Monte Carlo Filtering (MCF), a categorization is defined for each Monte Carlo realization based on whether the outputs fall into the target region B. One obtains two subsets of samples, $X_i|B$ and $X_i|\bar{B}$. The two-sample Kolmogorov-Smirnov (K-S) test can be performed to quantify the difference between the distributions of the two subsets of samples:

$$KS(X_i) = \sup|P_n(X_i|B) - P_{\bar{n}}(X_i|\bar{B})| \tag{4}$$

where $P_n(X_i|B)$ and $P_{\bar{n}}(X_i|\bar{B})$ are the empirical distribution functions of the two subsets of samples. The bigger $KS(X_i)$, the more important X_i is for the regionalised output. In addition, the p-value of K-S test quantifies the significance level of the null hypothesis, i.e. the two subsets of samples are from the same distribution.

Regional sensitivity analysis methods like MCF can be used to target the discrepancy. MCF is widely applied due to its easy implementation, where only a single set of Monte Carlo samples is required, and its straightforward filtering interpretation. However, compared with many global sensitivity analysis methods, MCF is not effective at revealing complex structures of parameter interactions and the contribution from products of parameters that might compensate [2]. Furthermore, as the K-S test from Eq.4 only quantifies the difference between the filtered and remaining samples, MCF cannot identify influential parameters within the target region.

Motivated by the effectiveness of filtering to target a specific region of interest, and the ability of global sensitivity analysis to identify influential parameters in a complex interaction structure, we propose a new regional sensitivity analysis approach that is a combination of the global Fisher information and the truncated distribution conditional on the measurement data.

3. Data driven sensitivity analysis using truncated Fisher information

In this section, we introduce the truncated Fisher Information Matrix (tFIM) to target directly the discrepancy. tFIM provides regional sensitivity information as the MCF. Nevertheless, a comparison between MCF and tFIM shows that parameter interactions can be better handled with the Fisher information metric. This will be illustrated numerically in Section 4 below.

3.1. Truncated Fisher Sensitivity Analysis

Consider a general vector function $\mathbf{y} = \mathbf{h}(\mathbf{x})\colon \mathbb{R}^d \to \mathbb{R}^m$, the probabilistic sensitivity analysis characterise the uncertainties of the output $\mathbf{y}$ that is induced by the random input $\mathbf{x}$. When the input can be described by parametric probability density functions (PDF), i.e., $x \sim p(\mathbf{x}|\mathbf{b})$, the Fisher Information Matrix (FIM) can then be estimated as the covariance matrix of the gradient vector of the joint PDF $\partial \ln p(\mathbf{y}|\mathbf{b})/\partial \mathbf{b}$, with the jk^{th} entry of the FIM as [20]:

$$F_{jk} = \int \frac{\partial p(\mathbf{y}|\mathbf{b})}{\partial b_j} \frac{\partial p(\mathbf{y}|\mathbf{b})}{\partial b_k} \frac{1}{p(\mathbf{y}|\mathbf{b})} d\mathbf{y} = \mathbb{E}_Y \left[\frac{\partial \ln p}{\partial b_j} \frac{\partial \ln p}{\partial b_k} \right] \tag{5}$$

where the quantity of interest (QoI) in our study could be the discrepancy between simulation and measurement, i.e. $\mathbf{y} = \mathbf{y_d}(\mathbf{x})$ from Eq.3. Note that the PDF of the QoI can be high dimensional, for example a frequency response with 100 frequency points would leads to a 100 dimensional joint PDF $p(\mathbf{y})$. Although high dimensional QoIs is not an issue in theory, estimation of its joint PDF is prohibitively inefficient for as low as 10 dimensions [21]. It is thus more tractable to consider a lower dimensional summary and this is discussed in Section 3.5.

In contrast to variance-based approaches which implicitly assume that output variance is a sensible measure of the output uncertainty, FIM can examine the perturbation of the entire joint PDF of the outputs. This is closely linked to the relative entropy between the PDF of the outputs and its perturbation due to an infinitesimal variation of the input distributions [22, 23].

Nevertheless, Fisher information based sensitivity analysis using Eq.5 cannot be used directly to target the discrepancy reduction, because the measured data does not depend on the parametrization of the simulation model. The dependency of the discrepancy term on the design parameters solely come from the simulated data.

Here we propose a data driven sensitivity analysis using truncated FIM (tFIM). The key insight here is that as the occurrence of the response is known to be within a specified range, via the observation of the measured data, truncated distributions can be utilised for sensitivity analysis targeting the discrepancy. The truncated distribution, which is a conditional distribution, can be expressed as:

$$p(\mathbf{y}_{\mathrm{T}}) = p(\mathbf{y}|\boldsymbol{\alpha} \le \mathbf{y} \le \boldsymbol{\beta}) = \frac{1}{Z} p(\mathbf{y}) \mathbf{I} \left[\boldsymbol{\alpha} \le \mathbf{y} \le \boldsymbol{\beta} \right] \tag{6}$$

where $\boldsymbol{\alpha} \le \mathbf{y} \le \boldsymbol{\beta}$ indicates $\{\alpha_n \le y_n \le \beta_n, n = 1, 2, \ldots, m\}$, and I is the indicator function. $Z = \int_{\alpha_m}^{\beta_m} \cdots \int_{\alpha_1}^{\beta_1} p(\mathbf{y}) \mathrm{d}\mathbf{y}$ is the normalisation constant.

The truncation region is dependent on the measured data, i.e. $\boldsymbol{\alpha} = \boldsymbol{\alpha}(\boldsymbol{\phi_m})$ and $\boldsymbol{\beta} = \boldsymbol{\beta}(\boldsymbol{\phi_m})$. The truncation thus directly targets the discrepancy $\mathbf{y_d}$ between our model simulation and the measurement.

The simulation function $\mathbf{y} = \mathbf{h}(\mathbf{x})$ can be seen as a transformation from the input random variables $\mathbf{x}$ to the output random variables $\mathbf{y}$. Therefore, the truncated distribution from Eq.6 can be further expressed as:

$$p(\mathbf{y}_\mathrm{T}|\mathbf{b}) = \frac{1}{Z}\int \prod_n \delta\left[y_n - h_n(\mathbf{x})\right] I\left(\alpha_n \leq h_n(\mathbf{x}) \leq \beta_n\right) p(\mathbf{x}|\mathbf{b})\mathrm{d}\mathbf{x} \tag{7}$$

where $\delta(\cdot)$ is the Dirac delta function. $\mathbf{b}$ are the distribution parameters of input design parameters. In cases the inputs $\mathbf{x} \in \mathbb{R}^d$ are described by Gaussian distributions, $\mathbf{b} \in \mathbb{R}^{2d}$ represent the mean and standard deviation of the distributions.

In our case, the quantity of interest is the discrepancy between simulation and measured data, i.e. $\mathbf{y_d} = \mathbf{h}(\mathbf{x})$. Therefore, the indicator function rejects simulations that have a large distance from the measured data, and plays the role of approximating the likelihood function. Eq.7 thus has the intuitive interpretation of a marginal likelihood, where the input uncertainties over $\mathbf{x}$ have been marginalised. As a result, sensitivity analysis using the truncated distribution $p(\mathbf{y}_\mathrm{T})$ can help to identify the main uncertainties to improve the agreement between the simulation and measurement.

It is noted in passing that the formulation in Eq.7 bears similarity to rejection based Approximate Bayesian Computation (ABC) methods (see e.g. [16]), where the likelihood is approximated using a distance function via simulations. However, while ABC aims to estimate the posterior distributions of the uncertain parameters in a Bayesian framework, our goal is to identify the dominant uncertainties for the discrepancy via sensitivity analysis. As mentioned, the advantage of sensitivity guided design verification over a direct updating is the potential to help the designers and engineers with an improved understanding of the causes of the discrepancies.

From the truncated distribution, which is conditional on the measurement data, the truncated Fisher information can be obtained similarly to Eq.5:

$$F_{\mathrm{T}_{jk}} = \int \frac{\partial p(\mathbf{y}_\mathrm{T})}{\partial b_j}\frac{\partial p(\mathbf{y}_\mathrm{T})}{\partial b_k}\frac{1}{\partial p(\mathbf{y}_\mathrm{T})}\mathrm{d}\mathbf{y}_\mathrm{T} \tag{8}$$

We follow a Monte Carlo (MC) based sampling approach to estimate the tFIM, where the components of the FIM can be estimated efficiently using the Likelihood Ratio method [24, 22]. More specifically, the truncated density function and its gradient with respect to the distribution parameters can be expressed as:

$$\begin{aligned} p(\mathbf{y}_\mathrm{T}) &= \frac{1}{Z}\int \prod_n \delta\left[y_n - h_n(\mathbf{x})\right] I\left(\alpha_n \leq h_n(\mathbf{x}) \leq \beta_n\right) p(\mathbf{x}|\mathbf{b})\mathrm{d}\mathbf{x} \\ &\approx \frac{1}{NZ}\sum_i \prod_n \delta\left[y_n - h_n(\mathbf{x}_i)\right] I\left(\alpha_n \leq h_n(\mathbf{x}_i) \leq \beta_n\right) \end{aligned} \tag{9}$$

$$
\begin{aligned}
\frac{\partial p(\mathbf{y}_\mathrm{T})}{\partial \mathbf{b}} &= \frac{1}{Z}\int \prod_n \delta\left[y_n - h_n(\mathbf{x})\right] I\left(\alpha_n \le h_n(\mathbf{x}) \le \beta_n\right) \frac{\partial p(\mathbf{x}|\mathbf{b})}{\partial \mathbf{b}} \frac{p(\mathbf{x}|\mathbf{b})}{p(\mathbf{x}|\mathbf{b})} \mathrm{d}\mathbf{x} \\
&\approx \frac{1}{NZ}\sum_i \prod_n \delta\left[y_n - h_n(\mathbf{x}_i)\right] I\left(\alpha_n \le h_n(\mathbf{x}_i) \le \beta_n\right) \frac{\partial \ln p(\mathbf{x_i}|\mathbf{b})}{\partial \mathbf{b}}
\end{aligned}
\tag{10}
$$

The efficiency comes from the fact that both $p(\mathbf{y}_\mathrm{T})$ and $\partial p(\mathbf{y}_\mathrm{T})/\partial \mathbf{b}$ can be estimated at the same time, because the term $\partial p(\mathbf{x}|\mathbf{b})/\partial \mathbf{b}$ is often known analytically. It is also clear from Eq.9 and 10 that, just as the MCF method, the derivatives of the function $\mathbf{h}(\mathbf{x})$ are not required for the sensitivity analysis. Note that the normalisation constant does not affect the relative sensitivity results so it is not required for the numerical estimation.

The tFIM can therefore be estimated similarly to the original FIM using the Likelihood Ratio method described above for sensitivity analysis [6]. Better still, the same set of simulated MC samples that have been used for uncertainty and sensitivity analysis can be used to form the tFIM without additional model runs. While this is efficient, the truncation, without additional model runs, inevitably results in a relative small number of valid samples. MCF has the same issue. In the next section, we will utilise the unique structure of the tFIM and apply a random truncation to mitigate this issue.

3.2. Truncation with a random threshold

Successful implementation of the tFIM, same as MCF, depends on the choice of the truncation region. Typically, choice of truncation involves a trade-off, where a larger region reduces estimation variability thanks to a larger sample size, but also increases misfit between the simulation and the measured data. Although this has to be treated on a case by case basis, setting a hard bound is rarely satisfactory as we don't wish to be over-confident in an inaccurate truncation. This issue can be overcome by a random truncation, as a form of uncertainty inflation that is often used in Bayesian inverse problems [25], to incorporate additional uncertainties due to a lack of confidence in the truncation model.

The unique structure of the tFIM allows a straightforward incorporation of a random truncation threshold. Assuming the truncation thresholds can be described by parametric probability distributions, i.e. $\epsilon \sim p(\epsilon|b_\epsilon)$, we can then augment the input uncertain parameters as $[\mathbf{x}, \boldsymbol{\epsilon}]$ and form the new conditional truncation distribution as:

$$
p(\mathbf{y}_\mathrm{T}) = \frac{1}{Z}\int \prod_n \delta\left[y_n - h_n(\mathbf{x})\right] I\left(\alpha_n(\boldsymbol{\epsilon}) \le h_n(\mathbf{x}) \le \beta_n(\boldsymbol{\epsilon})\right) p(\mathbf{x}|\mathbf{b}) p(\boldsymbol{\epsilon}|\mathbf{b}_\epsilon) \mathrm{d}\mathbf{x}\mathrm{d}\boldsymbol{\epsilon} \tag{11}
$$

where the estimation of the distribution gradient follows similarly from Eqs.9 and 10.

The truncated FIM is then augmented with extra dimensions that correspond to the uncertain truncation thresholds. The advantage of this approach is that the random thresholds are in the same space as the uncertain design parameters. The Fisher matrix then provides information of the interdependency between design parameters and the truncation thresholds, where a higher interaction would indicate greater influence of the corresponding design parameters for the truncated results.

Unlike the input design parameters of which the distributions are elicited and/or based on data collected, the distribution for the truncation thresholds can be specified based on the knowledge of the measured data and the preference for the truncation. In the case study presented in Section 5, an exponential distribution is used to truncate the discrepancy between simulated and measured data, giving preference to parameter values that agree better with measurement.

3.3. Fisher information based sensitivity indices

The sensitivity information from tFIM can be obtained similarly to the original FIM. For example, we know that a real symmetric FIM matrix $\mathbf{F}$ can be diagonalized by orthogonal matrices:

$$\mathbf{Q}^{-1}\mathbf{F}\mathbf{Q} = \mathbf{\Lambda} \tag{12}$$

where $\mathbf{Q}$ is the orthogonal eigenvector matrix, i.e. $\mathbf{Q}^\intercal = \mathbf{Q}^{-1}$, and $\mathbf{\Lambda} = \mathrm{diag}(\lambda_1, \lambda_2, \dots)$ contains the real eigenvalues. And the solution to Eq.12 can be solved using the standard eigenvalue equation:

$$\mathbf{F}\mathbf{Q} = \mathbf{Q}\mathbf{\Lambda}, \quad \text{with} \quad \det(\mathbf{F} - \lambda\mathbf{I}) = \mathbf{0} \tag{13}$$

The eigenvalues of the FIM represent the magnitudes of the sensitivities with respect to simultaneous variations of the parameters $\mathbf{b}$, and the relative magnitudes and directions of the variations are given by the corresponding eigenvectors [6].

In addition to the eigenvectors from the FIM, additional insights can be obtained using a Pythagorean view to estimate the contributions. In analogy to the principal component analysis, the contribution from the *ith* parameter can be estimated across different eigenvectors:

$$s_i = \sum_j^n q_{ij}^2 \lambda_j / \sum \lambda_j \tag{14}$$

where q_{ij} is the i_{th} element of the eigenvector $\mathbf{q}_j$, and the contribution has been normalised by the sum of eigenvalues.

Although the FIM sensitivity indices based on eigenvalues and eigenvectors are fundamentally different from Sobol' indices, Eq.14 can be used for parameter rankings so that different sensitivity methods can be directly compared as shown in [23]. Examples will be given in the numerical cases in Section 4 and the design case study in Section 5, in which we will not only show parameter rankings that use the complete set of eigenvectors, but also the results using only the dominant eigenvectors.

The contributions from different parameters of the same variables can be further aggregated for the corresponding variables, assuming the perturbations are independent. For example, if (b_j, b_k) are the mean and standard deviation of the variable x_m, then the sensitivity to the variable x_m can be obtained by adding the contributions of the parameters b_j and b_k.

As sensitivity analysis is often conducted following the uncertainty analysis, both FIM and tFIM can be estimated using the same set of Monte Carlo samples, i.e. one-sample set for both global and regional sensitivity analysis. This is same as MCF, but different from Sobol' where additional model runs are required.

3.4. Sensitivity with respect to the mean and standard deviation

tFIM needs to be normalised for sensitivity analysis. This is because the partial derivative vector $\partial \ln p/\partial b_j$ provides the relative effect on the perturbations for an infinitesimal change of b_j. However, these raw partial derivatives are not directly comparable when the parameters, b_j and b_k, are of different units. In addition, the FIM tends to be ill-conditioned without scaling because the parameters could be of many orders of magnitude different.

Different types of normalisation would suit different applications, but the standard deviation has been recommended as the normalisation constant for engineering design problems [6], implying the allowable range of parameter mean values is limited to the local region as quantified by the standard deviations.

To look at sensitivities with respect to the mean and standard deviation, the FIM and tFIM need to be re-parametrized. Suppose $b_j = g_j(\theta_i)$, $i = 1, 2, \ldots, s$, then the FIM with respect to the parameter $\boldsymbol{\theta}$ is [26]:

$$\mathbf{F}(\boldsymbol{\theta}) = \mathbb{J}^{\mathsf{T}}\mathbf{F}(\mathbf{b})\mathbb{J} \tag{15}$$

where $\mathbb{J}$ is the Jacobian matrix with $\mathbb{J}_{ji} = \partial b_j/\partial \theta_i$. The Jacobian parametrization matrices used in this paper are given in Appendix A.

Eq.15 can be used to transform the Fisher-based sensitivity analysis to a new set of parameters. For example, in the design case study in Section 5, we re-parametrize the sensitivities from the distribution parameters of Gumbel and Lognormal distributions to the means and standard deviations of the uncertain inputs.

3.5. Quantity of interest

Both the simulated response $\boldsymbol{\phi}(\omega, \mathbf{x})$ and the discrepancy $\mathbf{y_d}(\omega, \mathbf{x})$ become random vectors due to the presence of uncertainties in the parameters $\mathbf{x}$. As a result, the response at different frequencies tend to be correlated. For example, a change of damping would change the response at multiple frequencies at the same time. Therefore, looking at the probabilistic response at individual frequency points might be misleading.

In theory, it is possible to examine the joint PDF of the frequency response function. However, the joint PDF can be high dimensional, for example a frequency response with 1000 frequency points would leads to a 1000 dimensional joint PDF $p(\mathbf{y})$. Although high dimensional QoIs is not an issue in theory, estimation of its joint PDF is prohibitively inefficient [21]. A transformation of the frequency responses in Eq.1 to the modal coordinates can reduce the dimension if the modes are well separated, but it requires the damping being negligible or proportional. This high dimensional issue tends to get worse as it is common to measure the response at multiple spatial positions of a mechanical system where $\mathbf{y_d} = \mathbf{y_d}(\omega, \xi, \mathbf{x})$, with ξ indicating the measurement position.

Considering the complex nature of the frequency responses, in this case study, we average the frequency responses over frequencies and measurement positions, for the response magnitude (mag) and phase (pha) respectively:

$$\begin{aligned} y_d^{\text{mag}}(\mathbf{x}) &= \frac{1}{MN}\sum_i^M \sum_j^N \left| y_d^{\xi_i}(\omega_j, \mathbf{x}) \right| \\ y_d^{\text{pha}}(\mathbf{x}) &= \frac{1}{MN}\sum_i^M \sum_j^N \left| \angle y_d^{\xi_i}(\omega_j, \mathbf{x}) \right| \end{aligned} \tag{16}$$

where ω_j are the frequencies of interest and ξ_i are response positions. This allows us to form the 2-dimensional output quantity of interest below, irrespective of the number of frequency points and measurement positions:

$$\mathbf{y}(\mathbf{x}) = \begin{bmatrix} y_d^{\text{mag}}(\mathbf{x}) & y_d^{\text{pha}}(\mathbf{x}) \end{bmatrix} \tag{17}$$

The metric for the QoI in Eq.16 uses the mean absolute difference between simulation and measurement, which emphasizes the proportional contributions at each frequency and measurement point. This provides a good representation of the overall differences, and it is preferred in this case over the (root) mean square difference which tends to be dominated by a few large differences.

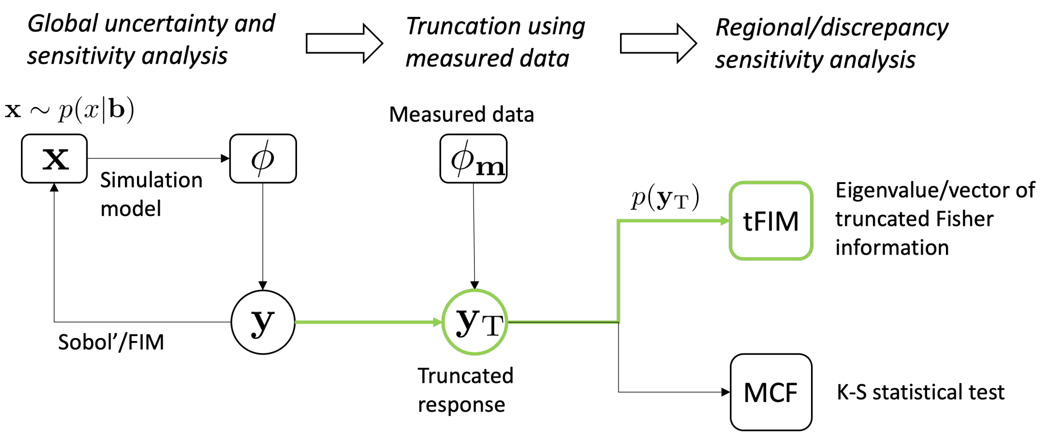

Figure 1: From global to regional sensitivity analysis to target design discrepancies between simulation and measurement. The development of the new truncated Fisher information is highlighted. Numerical demonstrations with Sobol', original FIM and MCF methods will be shown in comparison. Neither tFIM nor MCF require additional model runs.

An overview of the process from the global uncertainty and sensitivity analysis to the regional analysis to target the verification discrepancy is shown in Figure 1. As the estimation of both Sobol' and the Fisher information for global sensitivity analysis is Monte Carlo based, the regional sensitivity analysis using tFIM or MCF can then be estimated using the same set of samples at negligible additional computational costs.

In this paper, the TEDS toolbox [6] is utilised and modified for the estimation of tFIM, while the Sobol' indices have been calculated using the SAFE sensitivity toolbox [27]. For the vector QoI given in Eq.17, the aggregated Sobol' indices introduced in [28] are used:

$$GS_i = \frac{\sum_j Var(Y_j)S_i^j}{\sum_j Var(Y_j)} \quad GS_{T_i} = \frac{\sum_j Var(Y_j)S_{T_i}^j}{\sum_j Var(Y_j)} \tag{18}$$

where the S_i^j and $S_{T_i}^j$ are the 1st order and total order Sobol' indices for the jth output with respect to the ith input parameter. In our two-dimensional output case, $j = 1, 2$ corresponding to the magnitude and phase response respectively. $Var(Y)$ indicate the variance of outputs.

4. Numerical benchmark

As mentioned in the introduction, Sobol' indices are the benchmarks for global sensitivity analysis, while a commonly used approach for design verification is MCF. In this section, we will use two numerical examples to benchmark the proposed FIM based regional sensitivity indices against Sobol' and MCF. Two tractable examples are chosen. Despite its simplicity, these examples help to highlight the drawbacks of MCF and how the truncated FIM (tFIM) could help resolve these issues.

The two examples are listed in Table 1. Note that while Gaussian inputs are assumed in this section, a variety of distribution types, including Gumbel and Lognormal distributions, are considered in the design case study in Section 5.

Table 1: Distributions and target output regions for the two numerical benchmark cases. Gaussian distributions assumed for all inputs.

	Input distribution	Target output region
Case-1 $y = x_1 x_2$	$x_1 \sim \mathbb{N}(0, 0.15^2)$ $x_2 \sim \mathbb{N}(0, 0.15^2)$	$y \geq 0$
Case-2 $y = x_1 + x_2 + x_3$	$x_1 \sim \mathbb{N}(2, 1^2)$ $x_2 \sim \mathbb{N}(-2, 1^2)$ $x_3 \sim \mathbb{N}(0, 0.25^2)$	$-0.25 \leq y \leq 0.25$

Case-1 considers the product function $y = x_1 x_2$ with a target region of $y \geq 0$. In the design verification context, the target region is typically based on the measured data which would indicate non-negative outputs in this case. As the contributions to the target output from the two inputs tend to compensate for each other, as seen in Figure 2a from the scatter plot, MCF is expected to be challenged to identify their relative importance.

The results for Case-1 are shown in Figure 3, where it is clear that MCF fails to identify either of the two inputs as expected. In comparison, the proposed tFIM successfully identifies both x_1 and x_2 as influential and their equal importance.

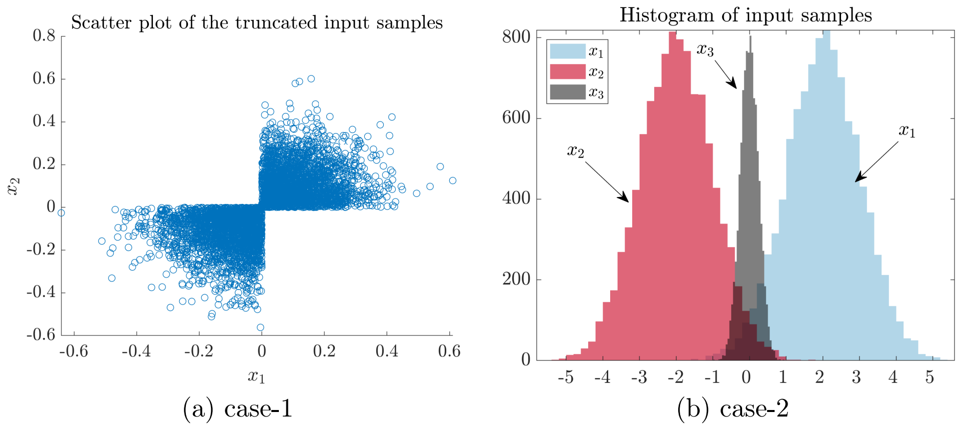

Figure 2: Example of input samples. (a) scatter plot of the input samples after truncation using $y \geq 0$; (b) histogram of the three inputs, highlighting the concentration of x_3 in the target region of $-0.25 \leq y \leq 0.25$.

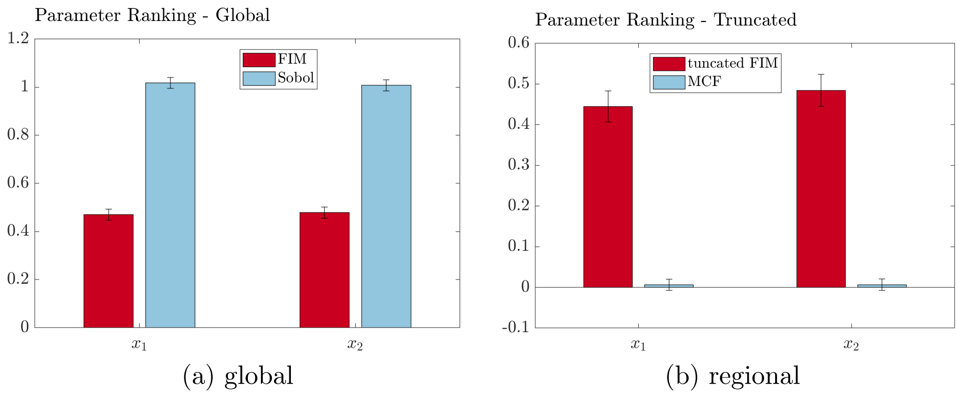

Figure 3: Sensitivity results for Case-1 $y = x_1 x_2$. (a) global SA with FIM and Sobol'; (b) regional SA with target region $y \geq 0$, using truncated FIM (tFIM) and Monte Carlo Filtering (MCF). Error bars indicate bootstrapping standard deviations: smaller the standard deviation, better convergence.

Case-2 considers a linear combination of three parameters, $y = x_1 + x_2 + x_3$, where the target output region is $-0.25 \leq y \leq 0.25$. In this case, as the presence of x_3 concentrates in the target region as seen in Figure 2b from the histogram plot, its effect in driving the outputs into the target region is minimal. As a result, x_3 will not be identified as important from MCF analysis, and this is clear from the sensitivity results shown in Figure 4b.

Nevertheless, within the target region, the contribution of x_3 is not negligible. Ideally the regional sensitivity analysis should also identify the effect of x_3 within the target region. It can be seen from Figure 4b that the tFIM results is different from MCF in this case. x_3 is not negligible according to tFIM, although its importance is relatively lower than x_1 and x_2.

In addition to overall parameter ranking, the decomposition of the tFIM matrix can

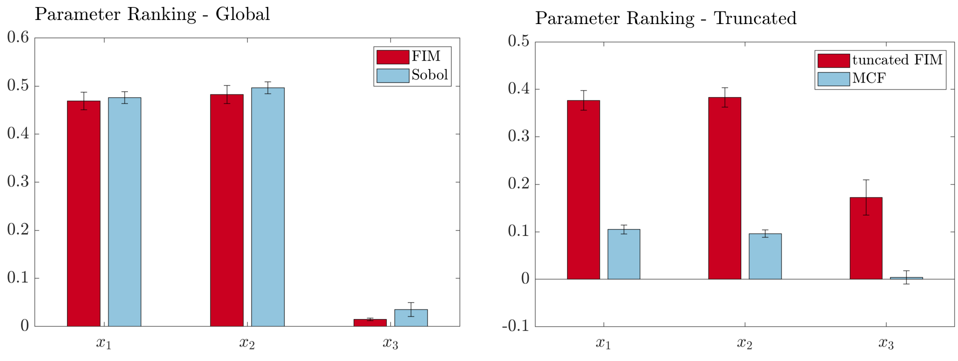

Figure 4: Sensitivity results for Case-2 $y = x_1 + x_2 + x_3$ and target output region is $-0.25 \le y \le 0.25$, same key as Figure 3.

provide additional sensitivity insights. The results for Case-2 is presented in Figure 5. The 1st eigenvector identifies high influence of the standard deviation (std dev) parameters of x_1 and x_2, while the 2nd eigenvector highlights the distinctive effect of x_3. It is therefore plausible to interpret that, the 1st eigenvector points to the directions in driving the output into the target region, while the 2nd eigenvector provide sensitivity information within the target region.

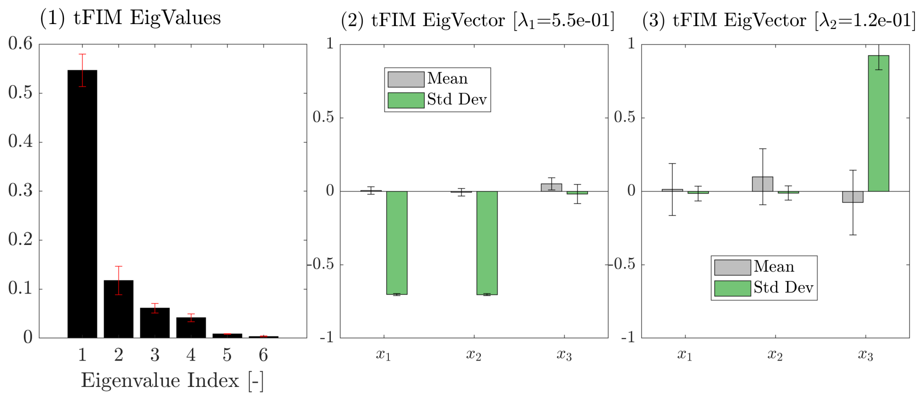

Figure 5: Case-2: decomposition of tFIM sensitivity results using eigenvalues and eigenvectors. (1) tFIM eigenvalues; (2) 1st eigenvector; (3) 2nd eigenvector.

Also shown in Figure 3a and Figure 4a are the global sensitivity results from Sobol' and FIM. The Sobol's total effect is given for Case-1 for this product function as the Sobol's main effect is zero, and vice versa for the sum function for Case-2. It can be seen that both methods have successfully identified the equal importance of x_1 and x_2 in both cases, and the negligible effect of x_3 for Case-2.

To check the convergence of the sensitivity indices, the bootstrapping method [29] is used. In bootstrapping, the input-output base samples are resampled randomly with replacement. For regional sensitivity analysis, bootstrapping might become unreliable due to small sample sizes [30], where low variation of un-influential parameters might be a false indicator of convergence. Although this is less a concern in our study, as the main objective is to identify influential design parameters, care should be taken when interpreting the absolute values of the bootstrapping uncertainties. The biggest advantage of bootstrapping is its efficiency, as no additional model runs are required. Throughout the numerical examples in this paper, 1000 bootstrappings are conducted and the resulting bootstrapping standard deviations are shown as error bars for each sensitivity indices.

5. Design verification of a model floating wind turbine tower

In this section, we apply the proposed tFIM to the design and testing of a model floating wind turbine. We first introduce the design verification problem in Section 5.1, where a floating column is designed representing a substructure of floating offshore wind turbines. In Section 5.2, we focus on the discrepancy between simulation and experiment, and make use of tFIM to identify the most influential parameters that are causing the discrepancy. In Section 5.3, the input parameters are augmented with random truncation thresholds for tFIM. This allows us to examine the interactions between the random parameters and identify the key discrepancy drivers with uncertain truncations. We demonstrate the design verification results in Section 5.4.

The simulation model for our case study has been developed using the CHAOS hydrodynamic code [31] which uses the semi-empirical Morison's equation [32] to estimate wave forces.

5.1. Design and testing

A design verification problem using a model floating column is studied, which represents a substructure of floating offshore wind turbines. As the floating configuration enables economic offshore wind electricity generation in deep waters, where fixed foundation turbines are not feasible, the chosen example is therefore pertinent to the renewable energy drive. In addition, due to the non-linear wave/structure interaction and the random wave environment, a simulation model is almost always required in the design of offshore structures.

Note that in this case study we have assumed the model structure in the wave tank is our full size design and have thus ignored any scalability issues. This is based on the consideration that the model used in simulation based design is typically full size. Nevertheless, the resulting model structure has its first natural frequency out of the wave frequency range, which is the same as typical offshore structures.

In this case study, a tethered model floating column is designed as shown in the schematic in Figure 6a and this is called the proposed design. The designed column is hollow and made of acrylic, as shown in Figure 6b. The metal ring corresponds to the 'Ballast 'indicated in Figure 6a, and the final developed design that is used for testing is shown in Figure 6c.

During the testing phase, we have conducted experiments for the wave response of the floating column in a wave tank that is 12 meter long and 0.5 meter wide. The waves were assumed to be one-dimensional in the wave tank. Both harmonic design waves, ranging from 0.5 Hz to 1.1 Hz, and random waves with Jonswap spectrum have been tested. The

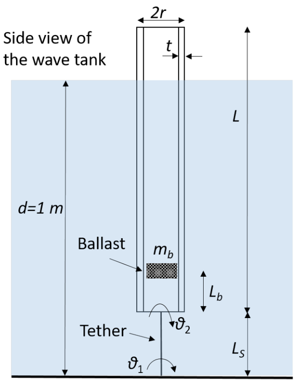

(a) Proposed design

(b) Column format

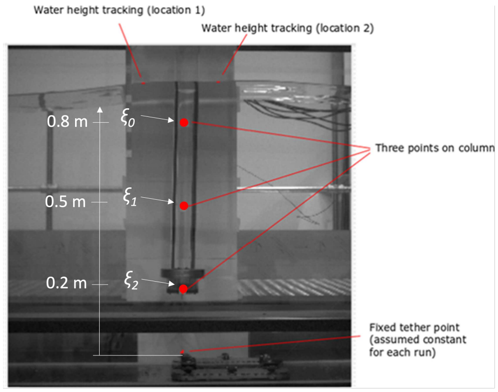

(c) Developed design

Figure 6: Design for the case study. (a) proposed design of the rig, consisting of a floating column in a wave tank; (b) picture of the designed acrylic column, 1 m length, 90 mm diameter, 2 mm wall thickness. It is tethered to the base of the tank and has removable metal rings, 'ballast', to alter the centre of gravity; (c) Developed design in wave tank for the testing. The three measurement positions are also indicated.

discussions in this paper will focus on the results from harmonic wave excitations, while future work will use the random wave data to explore the interaction between uncertain parameters and the stochastic wave states.

One of the challenges for the testing is to capture the motion of the floating structure. The application of conventional set up for fixed structures, such as the wired inertial measurement units, might interfere with the motion of the floating column. In this study, a non-intrusive image tracking system has been developed instead as shown in Figure 6c. Three different positions along the column have been tracked during wave excitation, with a sampling frequency of 40 Hz, to provide a good spatial coverage of the structural response. The coordinates of the three positions have been marked in Figure 6c. In addition, the wave heights on either side of the structure have also been monitored and that allows us to estimate the phase information of the harmonic wave responses (c.f. Figure 6c). The captured images, with Figure 6c showing one example frame, were then post-processed using the Lucas and Kanade algorithm [33] to extract the time history motion of the tracked positions. The data acquisition and the image post-processing has been set up using Labview from National Instruments.

5.2. Uncertainty and global sensitivity analysis

In the design verification problem of the model floating column, there are 15 input variables and their nominal design values are listed in Table 2. The uncertainties of the input parameters are obtained via elicitation and reference to the literature. For example, we use Gumbel distributions for the inertial and drag coefficients with coefficient of variation (CoV) of 0.1 for wind turbine design, and choose Lognormal and small CoV of 0.02 for many of

Table 2: Distributions for the input random variables of the floating column design, including Lognormal, Normal and Gumbel distributions. Nominal values and the Coefficient of Variation (CoV) of the parameters are also given.

	Material density	Water density	Water depth	Mass coefficient	Drag coefficient	Column length	Ballast mass	Ballast position
	ρ [kg/m3]	ρ_f [kg/m3]	d [m]	C_a [-]	C_d [-]	L [m]	m_b [kg]	L_b [m]
Distribution	Normal	Normal	Normal	Gumbel	Gumbel	Normal	Normal	Lognormal
Nominal	1600	1025	1	1	1	1.05	1.8	0.07
CoV	0.05	0.05	0.05	0.1	0.1	0.02	0.05	0.1
	TopCap mass	TopCap position	BottomCap mass	BottomCap position	Tether length	Column radius	Column thickness	
	m_{tc} [kg]	L_{tc} [m]	m_{bc} [kg]	L_{bc} [m]	L_s [m]	r [m]	t [m]	
Distribution	Normal	Normal	Normal	Lognormal	Lognormal	Lognormal	Lognormal	
Nominal	0.41	1.05	0.41	0.01	0.2	4.5e-2	2e-3	
CoV	0.05	0.05	0.05	0.05	0.1	0.02	0.02	

well specified dimensions like L, r and t [34].

With the input data given in Table 2, we first conduct global sensitivity analysis using the standard Fisher Information Matrix with 10000 MC samples. The results for parameter ranking are show in Figure 7, where the FIM results are compared to Sobol'. 1000 bootstrapping are used to verify the convergence of the resulting sensitivity indices.

From Figure 7, it can be seen that Sobol' total index (Sobol-Total) and FIM with all eigenvectors (All FIM-EigV) provide similar sensitivity results, by identifying the water depth d, water density ρ_f, tether length L_s and column radius r as the more influential design parameters. Similarly, Sobol' first order or main effect index (Sobol-Main) and FIM with the 1st eigenvector (1st FIM-EigV) provide similar sensitivity results, except that d is seen as the dominant from these two sensitivity indices.

The biggest issue with Sobol' is the heavy computational requirement. In this case, 10,000 samples are used for FIM. For Sobol', the same 10000 samples is used as the base. Since Sobol' indices are proportional to the input dimension, a total of $10000 \times (15 + 1)$ is required in this case where 15 is dimension of input parameters.

Despite the large number of samples required, the Sobol' results haven't completely converged, evidenced by the larger bootstrapping standard deviation and negative sensitivity values for some of the parameters. It should be noted that however that Sobol' indices are more quantitative which can be desirable in cases where the exact uncertainty reduction is required.

Results from Figure 7 help identify the most influential parameters of the design under uncertainties. This global information can guide the design and development to reduce uncertainties and improve the design. However, with testing data for design verification, a more targeted sensitivity analysis can be conducted using tFIM and MCF methods. As both

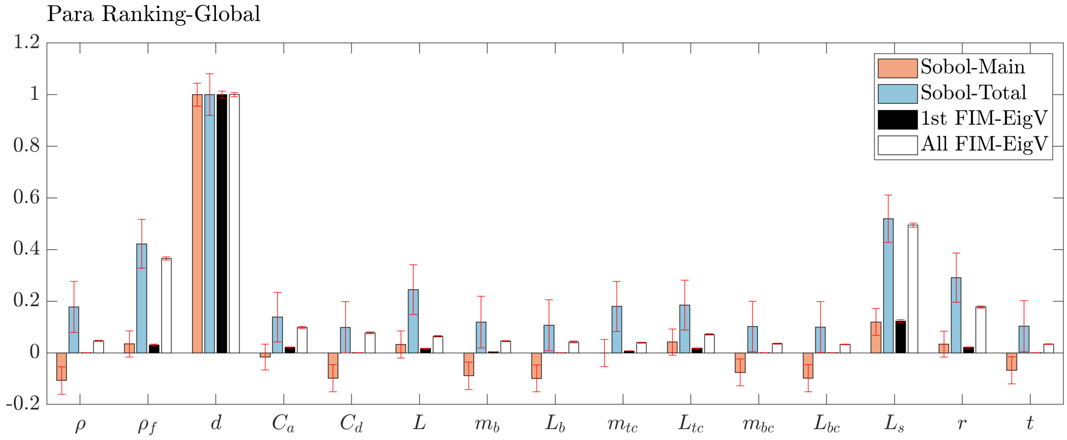

Figure 7: Global sensitivity parameter ranking for the model floating column design, with inputs from Table 2, from FIM and Sobol' methods. Relative ranking is shown here where the largest values from different methods are normalised, as absolute values of the results from FIM and Sobol' are not directly comparable. For FIM, two cases are considered where one case uses only the 1st eigenvector and the other case uses all eigenvectors.

methods can make use of existing samples, there is no additional computational cost but additional insights to reduce the discrepancy between the simulation and experiment may be obtained.

5.3. Discrepancy sensitivity analysis

The global sensitivity results from Figure 7 help identify the most influential parameters of the design, and guide the design and development to reduce uncertainties. With testing data for design verification, however, a more targeted sensitivity analysis can be conducted using tFIM and MCF methods. As both methods can make use of existing samples, there is no additional computational cost but additional insights to reduce the discrepancy between the simulation and experiment may be obtained.

In Figure 8, the simulated response is compared with the measured data at each of the three positions. The amplitude of the measured frequency response is extracted from the peak value of 20 cycles time history data at each wave frequency. The dashed line describing the amplitudes in Figure 8 then indicate the mean value from the 20 cycles and the error bars provide the corresponding standard deviations.

The measured amplitudes were found to be consistent as evident from the small error bars, which reflects the validity of the image tracking system described in Section 5.1. The phase information of the measured frequency response is based on the phase of the cross power spectral density, between the time history data at the three positions and the measured wave height. The averaged value of the data from the two wave tracking positions, shown in Figure 6c, is used. The measured phase information is not as reliable as the corresponding amplitudes because the wave height tracking was found to fluctuate. This might have caused the oscillations for the phase data shown in Figure 8, which nevertheless provides valuable validation for the simulation.

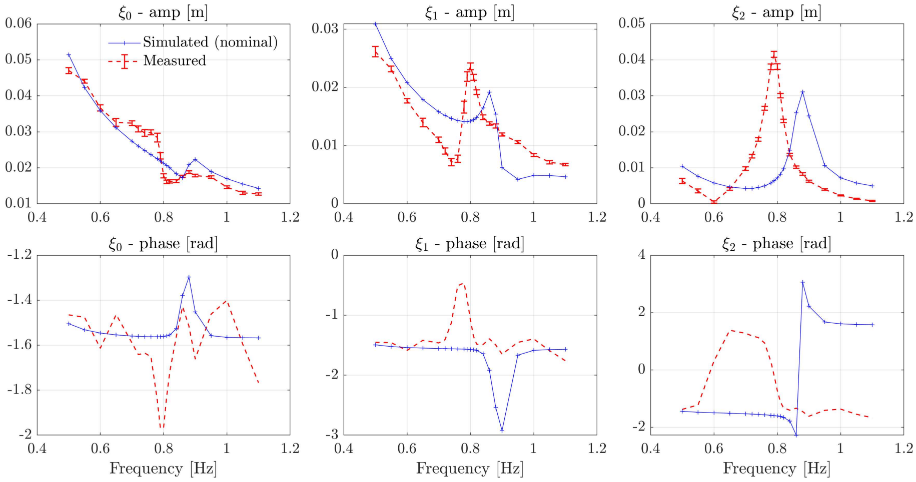

Figure 8: Comparison between measurement and simulation with the nominal input data at the 3 measurement positions. Top row shows the magnitude of the response and the bottom rows for the phase information.

The regional sensitivity results using the discrepancy between simulated and measured data are shown in Figure 9. Both tFIM and MCF results depend on the window of truncation. For smaller truncation windows, the experimental data is more accurately targeted but the statistical power is reduced for sensitivity analysis as fewer samples are chosen. For bigger windows, the effect is reversed.

Bootstrapping can help to verify the convergence of the results and 1000 bootstrapping resampling has been used for the results in Figure 9. We follow the ABC literature [35] and use a quantile based based strategy for setting the tolerance value. We use 5% of the total samples (500 samples) that are nearest to the experimental observation as the truncated . The same truncation data is used for both for tFIM and MCF estimations. One example of the simulated spectrum from the truncated samples is shown in Figure 10.

From Figure 9, similar sensitivity results are obtained from both MCF and tFIM. Recall that tFIM can potentially provide additional information about parameter interactions and the sensitivity within the truncated region, and this helps to explain the difference in terms of some of the parameters, such as C_a and C_d which also have contributions to the output uncertainty as seen from Sobol' total indices in Figure 7. In addition, for tFIM, the overall parameter ranking can be decomposed and sensitivity information from its dominant eigenvectors provides additional insight about the influential parameters and their interactions. For example, in this case, the water depth d dominates the 1st eigenvector and that is for both the mean and std of d.

5.4. tFIM with random truncation thresholds

The regional sensitivity results depend on the window of truncation. Setting the bounds requires a trial and error approach and the resulting truncation can greatly impact the sensitivity results from both MCF and tFIM methods described in the previous section. In

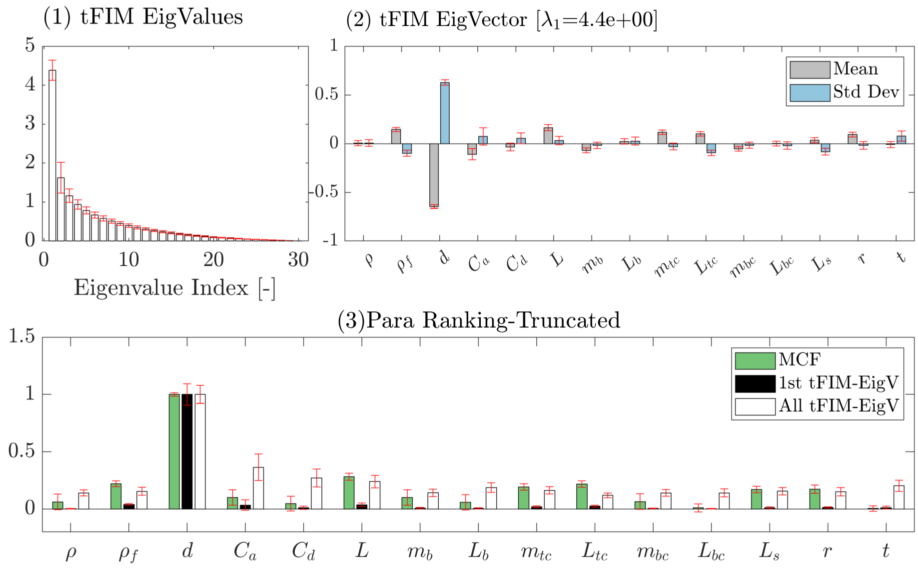

Figure 9: Sensitivity analysis for simulation measurement discrepancy using tFIM. (1) The eigenvalues of tFIM, where the 1st eigenvalue dominates; (2) 1st eigenvector of tFIM with respect to the mean and standard deviation (std dev) of the input parameters; (3) Parameter ranking using tFIM and MCF, where the biggest values from different methods are normalised to one. For tFIM, two cases are considered where one case uses only the 1st eigenvector and the other case uses all eigenvectors. The results are from 1000 bootstrapping, where the bars indicate the averaged results and the errorbars are for the bootstrapping standard deviations.

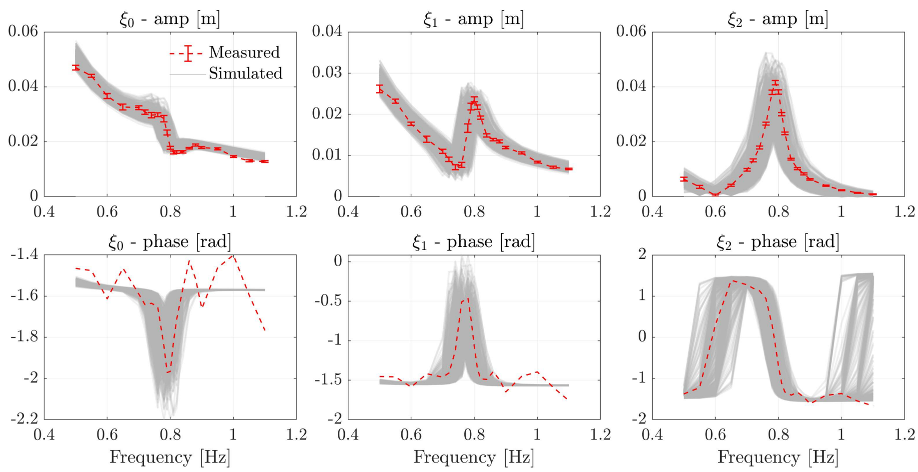

Figure 10: Indication of the simulated spectrum after truncation, compared with measured data. 5% of the total samples, 500 samples in this case, that are nearest to the experimental data are used for truncation. This is the same for tFIM and MCF methods.

this section, we augment the input random parameters and conduct tFIM sensitivity analysis with random truncation thresholds.

Exponential distributions are assigned for the truncation thresholds, of which the rate

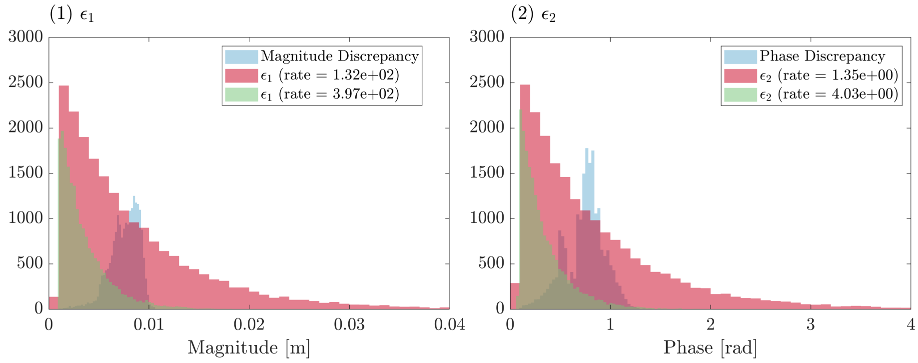

Figure 11: Histograms of the discrepancies between simulation and measurement, and the fitted Exponential Distributions for the random truncation thresholds. Two different rate parameters are considered for the random truncation, with the larger one 3 times bigger. (1) Magnitude discrepancy; (2) Phase discrepancy.

parameters are obtained by fitting exponential distributions to the discrepancy distributions for the magnitude and phase responses separately, as shown in Figure 11. Using exponential distributions for the truncation reflects our preference to the simulation results close to the measured data. The rate of decay controls the level of preference. Two different rate parameters are considered for the random truncation, with the larger one 3 times bigger.

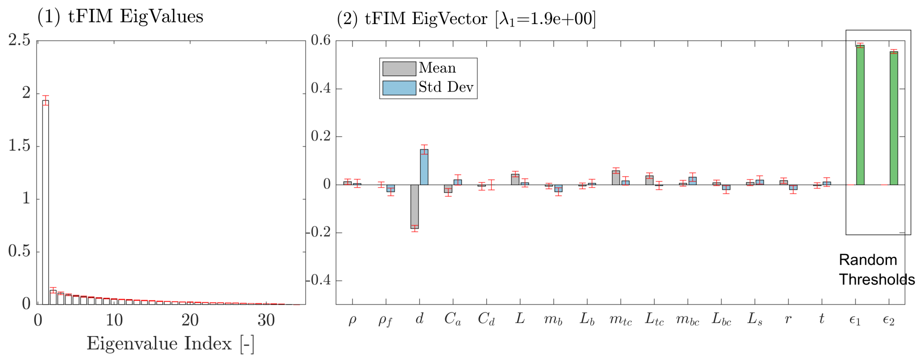

Figure 12: tFIM sensitivity analysis with random truncation. The input parameters are augmented with ϵ_1, the random threshold for magnitude, and ϵ_2, the random threshold for phase response. The 1st tFIM eigenvector shows the most influential interactions among the parameters. The results here are for the exponential distribution with a small rate parameter. Results for a larger rate are shown in Figure 13

The sensitivity results from tFIM with the augmented inputs is shown in Figure 12. In this case, the 1st eigenvalue dominates the sensitivity results and it is clear that the rate parameters of the random thresholds are most influential as expected. More importantly, the results provide an indication of the interaction structure between the truncation thresholds and the uncertain parameters for the design. In this case, it is clear that the water depth d has the strongest interaction with truncation thresholds.

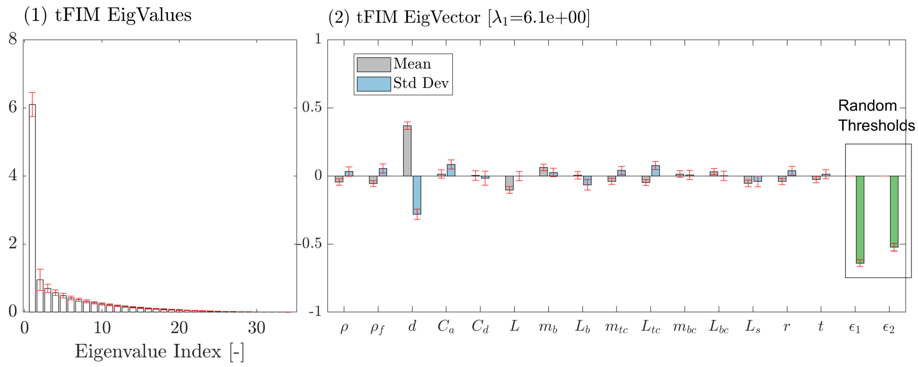

Figure 13: same key as Figure 12, but for the exponential distributed random thresholds with bigger rate parameters from Figure 11

The directly fitted exponential distribution has a relatively small rate parameter. This might result in negligible truncation effect. To investigate this further, we increase the original rate parameter by a factor of 3, resulting in a much concentrated truncation as shown in Figure 11. The corresponding tFIM result is shown in Figure 13. Similar conclusions can be drawn where the random truncation thresholds interact most strongly with the water depth d.

5.5. Summary

The magnitudes of the simulated response with nominal input values shown in Figure 8 are in reasonable agreement with the measurement. However, the phase results clearly deviates from the measured response even ignoring the oscillations. A common approach to improve the agreement is to tune the simulation parameters until the model matches the measurement better. In the presence of uncertainties, a Bayesian updating can be conducted, where the posterior distributions of the design parameters are obtained given the measurement data.

Utilising existing MC samples from uncertainty analysis, the samples that minimise the discrepancy could be identified and this would represent a point estimate for the nominal values of the uncertain design parameters. This best-fit, whose spectrum simulation is shown in Figure 14, involves updating a large subset of the design parameters as shown in Figure 15. In addition to potential over-fitting, more importantly, it provides little insight into the cause of the discrepancy, which is critical for design verification.

With the sensitivity information to the uncertainties of the model parameters, what could be done instead is to re-examine the discrepancies between the model and the design before model updating. For example, through the global and regional sensitivity analysis using the FIM, the water depth d has been identified as the most influential parameter. Sensitivity guided (SA guided) analysis significantly improves the agreement as shown in Figure 14, for both the amplitude and phase at all three positions. Importantly, the SA guided update is parsimonious, as shown in Figure 15, and provides explainable cause for the discrepancies.

The sensitivity analysis from the proposed tFIM provides us with guidance to focus on a subset of all parameters to reduce the discrepancy. In this case, tFIM analysis highlights the

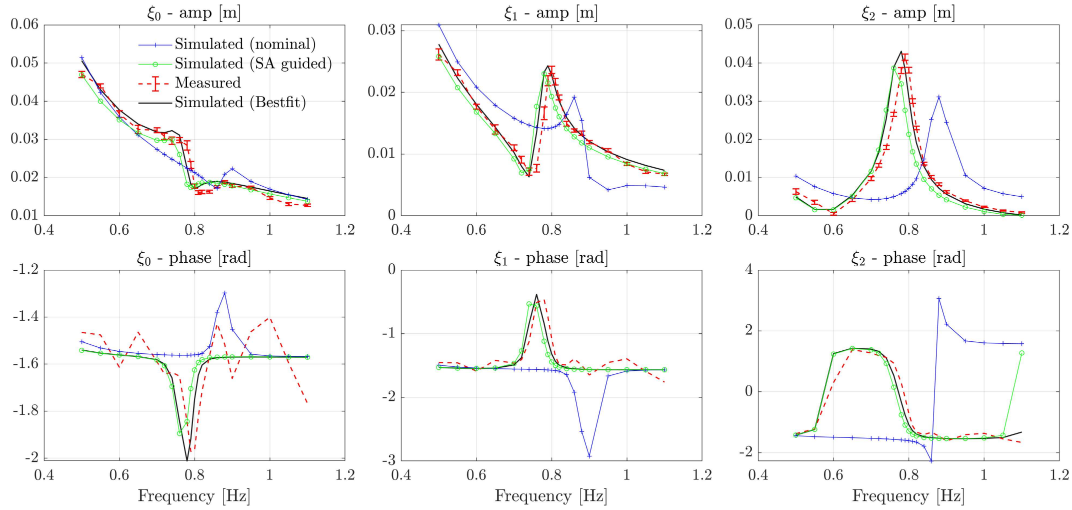

Figure 14: Comparison between measured and simulated response. Three different simulated results. Nominal result uses the nominal values of the inputs listed in Table 2; Best fit uses the sample, out of 10000 model evaluations, that minimise the discrepancy. The relative change of the nominal values is shown in Figure 15; SA guided result is based on 6% change of the water depth, as guided by the sensitivity analysis described in the previous sections.

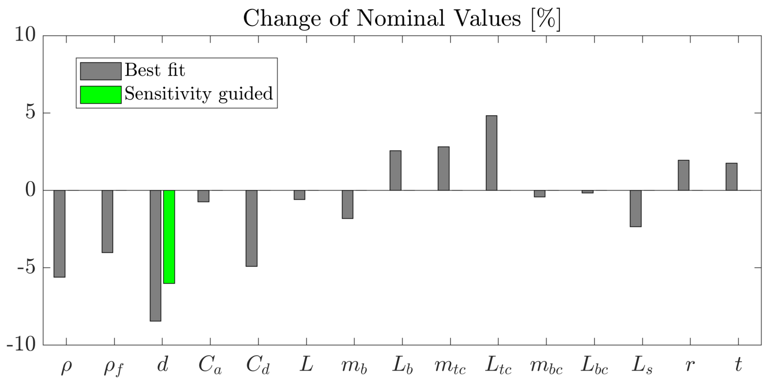

Figure 15: Percentage change of the nominal values of the input parameters.

distinctive importance of the water depth, using either fixed or random truncation. After re-examination of the design, it was found that the equivalent water depth in the water tank was shallower, for 0.06 m or 6% of the nominal depth, because of the presence of the tether fixture baseplate at the bottom of the wave tank as can be seen in Figure 6c.

The mismatches in the design or development set up can be a major source of uncertainty. Various types of mismatches between simulation and design set up can be easily overlooked in practice due to different focus of view between the simulation team and the design team [36]. For example, in this case study the base offset due to the installation of the tether fixture, as shown in Figure 6c, has been neglected in our initial examination of the developed design. This is because the base plate fixture does not affect the fixed boundary condition of the proposed design, and it was deemed negligible, based on engineering judgement by the design team. Sensitivity analysis using tFIM helps to focus on this small offset, which otherwise could have a significant (confounding) effect on the dynamic response.

Note that the comparison in Figure 15 only considers the nominal values, assuming the dispersion of the design parameters are unchanged. Following the sensitivity-guided reduction of discrepancy, a natural next step is to estimate the posterior distributions of the design parameters, using techniques such as Bayeisan updating. However, that further step is not considered in this paper, as our main purpose is to highlight the potential benefits of using sensitivity analysis, at no additional cost following a Monte Carlo based uncertainty analysis, to examine and reduce the discrepancies.

6. Conclusions

We present a new data-driven sensitivity analysis method based on the truncated Fisher Information Matrix (tFIM) to identify the key drivers of the discrepancy between simulation and measured data in the presence of uncertainties. Application of tFIM to the design verification of a model floating wind turbine successfully identified the single most important parameter out of 15 input random variables, and the sensitivity guided update is parsimonious and has clear physical interpretation.

tFIM is as efficient as the Monte Carlo Filtering (MCF), where the same set of samples from the preceding uncertainty analysis can be re-used. This is different from Sobol' indices where additional model runs are required in addition to the base samples. The one-sample approach means both tFIM and MCF essentially provide free regional sensitivity information targeting the verification data. The results from tFIM are found to be similar to MCF for the model floating column case study. Nevertheless, numerical examples show that tFIM can handle more complex parameter interaction structures and can additionally identify the influential parameters within the truncated region.

Both MCF and tFIM suffer from a small sample size due to the truncation. Although a larger number of base samples can potentially mitigate this issue, there is no guarantee of improvement if the model or experiment is biased. The structure of tFIM allows a natural incorporation of random truncations where the input parameters are augmented with the random truncation thresholds. Results show that the key drivers of discrepancy tend to have strong interactions with the random thresholds, and that provides a more robust strategy as no arbitrary fixed bound is assumed for the truncation.

Likelihood function is a widely used and principled way to combine a model and data, assessing how well the model fits the data. In cases the likelihood function is intractable or too expensive to compute but simulating data from the model is feasible, ABC-type methods can be used. tFIM does not assume the form of the likelihood function, as it makes approximations using a distance function via simulations, similar to rejection based ABC methods. However, truncation with a fixed bound discard data outside the specified range, which can lead to bias and misrepresentation. Using a random truncation in tFIM can mitigate this issue, though the need for a probabilistic model to define the truncation may introduce additional bias. Since random truncation in tFIM serves a role similar to probabilistic kernels in ABC, a promising direction for future research is to explore kernel-based approaches to examine the fundamental properties of tFIM and expand sensitivity analysis across a broader range of random truncation strategies.

The Fisher sensitivity is based on a joint PDF of the potentially multidimensional quantities of interest. This allows us to identify the influential variables that are important to the multidimensional responses simultaneously. In this paper, we have limited the analysis to a 2-dimensional output, namely the magnitude and phase of the complex frequency responses. This can have general applicability for the design of mechanical systems, but information at multiple frequency points and measurement positions have to be compressed. A future step is to explore options to examine a higher dimensional joint PDF for a more explicit analysis of the frequency response functions.

Acknowledgment

For the purpose of open access, the author has applied a Creative Commons Attribution (CC BY) licence to any Author Accepted Manuscript version arising. We thank Dr Robin Mills from the Laboratory for Verification and Validation (LVV), University of Sheffield, for his help on the experiment and sharing the testing data, and Prof Robin Langley, University of Cambridge, for helpful discussions and comment on an early draft. Part of this work has been funded by the Engineering and Physical Sciences Research Council through the award of a Programme Grant "Digital Twins for Improved Dynamic Design", Grant No. EP/R006768.

References

[1] Homma, Toshimitsu ; Saltelli, Andrea: Importance measures in global sensitivity analysis of nonlinear models. In: *Reliability Engineering & System Safety* 52 (1996), Nr. 1, 1-17. http://dx.doi.org/https://doi.org/10.1016/0951-8320(96)00002-6. – DOI https://doi.org/10.1016/0951–8320(96)00002–6. – ISSN 0951–8320

[2] Saltelli, A.: *Global sensitivity analysis: the primer*. John Wiley, 2008 http://books.google.at/books?id=wAssmt2vumgC. – ISBN 9780470059975

[3] Chen, Wei ; Jin, Ruichen ; Sudjianto, Agus: Analytical Variance-Based Global Sensitivity Analysis in Simulation-Based Design Under Uncertainty. In: *Journal of Mechanical Design* 127 (2004), 12, Nr. 5, 875-886. http://dx.doi.org/10.1115/1.1904642. – DOI 10.1115/1.1904642. – ISSN 1050–0472

[4] Opgenoord, Max M. J. ; Allaire, Douglas L. ; Willcox, Karen E.: Variance-Based Sensitivity Analysis to Support Simulation-Based Design Under Uncertainty. In: *Journal of Mechanical Design* 138 (2016), 09, Nr. 11. http://dx.doi.org/10.1115/1.4034224. – DOI 10.1115/1.4034224. – ISSN 1050–0472. – 111410

[5] Liu, Huibin ; Chen, Wei ; Sudjianto, Agus: Relative Entropy Based Method for Probabilistic Sensitivity Analysis in Engineering Design. In: *Journal of Mechanical Design* 128 (2005), 04, Nr. 2, 326-336. http://dx.doi.org/10.1115/1.2159025. – DOI 10.1115/1.2159025. – ISSN 1050–0472

[6] Yang, Jiannan ; Langley, Robin S. ; Andrade, Luis: Digital twins for design in the presence of uncertainties. In: *Mechanical Systems and Signal Processing* 179 (2022), November, 109338. http://dx.doi.org/10.1016/j.ymssp.2022.109338. – DOI 10.1016/j.ymssp.2022.109338. – ISSN 0888–3270

[7] Critchfield, Gregory C. ; Willard, Keith E.: Probabilistic analysis of decision trees using Monte Carlo simulation. In: *Medical Decision Making* 6 (1986), Nr. 2, S. 85–92

[8] Jia, Gaofeng ; Taflanidis, Alexandros A.: Sample-based evaluation of global probabilistic sensitivity measures. In: *Computers & Structures* 144 (2014), 103-118. http://dx.doi.org/https://doi.org/10.1016/j.compstruc.2014.07.019. – DOI https://doi.org/10.1016/j.compstruc.2014.07.019. – ISSN 0045–7949

[9] Borgonovo, Emanuele ; Plischke, Elmar: Sensitivity analysis: A review of recent advances. In: *European Journal of Operational Research* 248 (2016), Nr. 3, 869-887. http://dx.doi.org/https://doi.org/10.1016/j.ejor.2015.06.032. – DOI https://doi.org/10.1016/j.ejor.2015.06.032. – ISSN 0377–2217

[10] Zentner, Irmela ; Tarantola, Stefano ; de Rocquigny, E.: Sensitivity analysis for reliable design verification of nuclear turbosets. In: *Reliability Engineering & System Safety* 96 (2011), Nr. 3, 391-397. http://dx.doi.org/https://doi.org/10.1016/j.ress.2010.10.005. – DOI https://doi.org/10.1016/j.ress.2010.10.005. – ISSN 0951–8320

[11] Lucay, F. ; Cisternas, L.A. ; Gálvez, E.D.: Global sensitivity analysis for identifying critical process design decisions. In: *Chemical Engineering Research and Design* 103 (2015), 74-83. http://dx.doi.org/https://doi.org/10.1016/j.cherd.2015.06.015. – DOI https://doi.org/10.1016/j.cherd.2015.06.015. – ISSN 0263–8762. – Inventive Design and Systematic Engineering Creativity

[12] Østergård, Torben ; Jensen, Rasmus L. ; Maagaard, Steffen E.: Early Building Design: Informed decision-making by exploring multidimensional design space using sensitivity analysis. In: *Energy and Buildings* 142 (2017), 8-22. http://dx.doi.org/https://doi.org/10.1016/j.enbuild.2017.02.059. – DOI https://doi.org/10.1016/j.enbuild.2017.02.059. – ISSN 0378–7788

[13] Morris, Max D.: Factorial Sampling Plans for Preliminary Computational Experiments. In: *Technometrics* 33 (1991), Nr. 2, 161-174. http://dx.doi.org/10.1080/00401706.1991.10484804. – DOI 10.1080/00401706.1991.10484804

[14] Ratto, Marco ; Tarantola, Stefano ; Saltelli, Andrea: Sensitivity analysis in model calibration: GSA-GLUE approach. In: *Computer Physics Communications* 136 (2001), Nr. 3, S. 212–224

[15] Beven, Keith ; Binley, Andrew: The future of distributed models: model calibration and uncertainty prediction. In: *Hydrological processes* 6 (1992), Nr. 3, S. 279–298

[16] Turner, Brandon M. ; Van Zandt, Trisha: A tutorial on approximate Bayesian computation. In: *Journal of Mathematical Psychology* 56 (2012), Nr. 2, S. 69–85

[17] Mottershead, JE ; Mares, C ; Friswell, MI ; James, S: Selection and updating of parameters for an aluminium space-frame model. In: *Mechanical Systems and Signal Processing* 14 (2000), Nr. 6, S. 923–944

[18] Yuan, Zhaoxu ; Liang, Peng ; Silva, Tiago ; Yu, Kaiping ; Mottershead, John E.: Parameter selection for model updating with global sensitivity analysis. In: *Mechanical Systems and Signal Processing* 115 (2019), S. 483–496

[19] Mottershead, John E. ; Link, Michael ; Friswell, Michael I. ; Schedlinski, Carsten: Model updating. In: *Handbook of experimental structural dynamics* (2020), S. 1–53

[20] Cover, Thomas M. ; Thomas, Joy A.: *Elements of Information Theory*. Hoboken, UNITED STATES : John Wiley & Sons, Incorporated, 2006 http://ebookcentral.proquest.com/lib/cam/detail.action?docID=266952. – ISBN 978–0–471–74881–6

[21] Wasserman, Larry: *All of Statistics*. New York : Springer-Verlag, 2004

[22] Yang, Jiannan: A general framework for probabilistic sensitivity analysis with respect to distribution parameters. In: *Probabilistic Engineering Mechanics* 72 (2023), S. 103433

[23] Yang, Jiannan: Decision-oriented two-parameter Fisher information sensitivity using symplectic decomposition. In: *Technometrics* 66 (2024), Nr. 1, S. 28–39

[24] Spall, James C.: *Introduction to stochastic search and optimization: estimation, simulation, and control*. John Wiley & Sons, 2005

[25] Calvetti, Daniela ; Dunlop, Matthew ; Somersalo, Erkki ; Stuart, Andrew: Iterative updating of model error for Bayesian inversion. In: *Inverse Problems* 34 (2018), Nr. 2, S. 025008

[26] Lehmann, E. L. ; Casella, George: *Theory of point estimation*. 2nd ed. New York : Springer, 1998

(Springer texts in statistics). – ISBN 978–0–387–98502–2
[27] Pianosi, Francesca ; Sarrazin, Fanny ; Wagener, Thorsten: A Matlab toolbox for global sensitivity analysis. In: *Environmental Modelling & Software* 70 (2015), S. 80–85
[28] Gamboa, Fabrice ; Janon, Alexandre ; Klein, Thierry ; Lagnoux, Agnès: Sensitivity indices for multivariate outputs. In: *Comptes Rendus. Mathématique* 351 (2013), Nr. 7-8, S. 307–310
[29] Efron, Bradley ; Tibshirani, Robert J.: *An introduction to the bootstrap.* Chapman and Hall/CRC, 1994
[30] Sarrazin, Fanny ; Pianosi, Francesca ; Wagener, Thorsten: Global Sensitivity Analysis of environmental models: Convergence and validation. In: *Environmental Modelling & Software* 79 (2016), S. 135–152
[31] Yang, Jiannan: *Code for Hydrodynamic Analysis of Offshore Structures (CHAOS).* `https://github.com/longitude-jyang/hydro-suite/blob/856be1c70964a84afdc774cfd4a4aa0cbfdc5b00/CITATION.cff`. Version: Januar 2022. – 10.5281/zenodo.5831833
[32] Sarpkaya, Turgut '.: *Wave Forces on Offshore Structures.* Cambridge University Press, 2010. `http://dx.doi.org/10.1017/CBO9781139195898`. `http://dx.doi.org/10.1017/CBO9781139195898`
[33] Lucas, Bruce D. ; Kanade, Takeo: An Iterative Image Registration Technique with an Application to Stereo Vision. In: *Proceedings of the 7th International Joint Conference on Artificial Intelligence - Volume 2.* San Francisco, CA, USA : Morgan Kaufmann Publishers Inc., 1981 (IJCAI'81), S. 674–679
[34] Ramezani, Mahyar ; Choe, Do-Eun ; Heydarpour, Khashayar ; Koo, Bonjun: Uncertainty models for the structural design of floating offshore wind turbines: A review. In: *Renewable and Sustainable Energy Reviews* 185 (2023), S. 113610
[35] Beaumont, Mark A. ; Zhang, Wenyang ; Balding, David J.: Approximate Bayesian computation in population genetics. In: *Genetics* 162 (2002), Nr. 4, S. 2025–2035
[36] Maier, A. M. ; Kreimeyer, M. ; Lindemann, U. ; Clarkson, P. J.: Reflecting communication: a key factor for successful collaboration between embodiment design and simulation. In: *Journal of Engineering Design* 20 (2009), Nr. 3, 265-287. `http://dx.doi.org/10.1080/09544820701864402`. – DOI 10.1080/09544820701864402

Appendix A Parameter re-parametrization examples

The FIM and tFIM can be re-parametrised using Eq.15. In the numerical examples, the sensitivity results have been re-parameterised with respect to the (arithmetic) means (μ) and standard deviations (σ) of the inputs. In this case, we need to find $\partial b_j/\partial \mu_j$ and $\partial b_j/\partial \sigma_j$ for each b_j. Below, we demonstrate how to find the Jacobian transformation matrix for Gumbel and Lognormal distributions used in this paper.

- Gumbel distribution

  Assume the input follows a Gumbel distrbution, with $x \sim \mathtt{Gum}(b_1, b_2)$ where b_1 is the location and b_2 is the scale. Then the two parameters can be expressed using its mean ad standard deviation as:

  $$b_1 = \mu - \sqrt{6}\gamma/\pi\sigma; \quad b_2 = \sqrt{6}\pi\sigma \tag{A.1}$$

  where γ is the Euler–Mascheroni constant. From Eq.A.1, the Jacobian matrix for re-parameterization can be formed as:

  $$\mathbb{J} = \begin{bmatrix} \frac{\partial b_1}{\partial \mu} & \frac{\partial b_1}{\partial \sigma} \\ \frac{\partial b_2}{\partial \mu} & \frac{\partial b_2}{\partial \sigma} \end{bmatrix} = \begin{bmatrix} 1 & -\sqrt{6}\gamma/\pi \\ 0 & \sqrt{6}/\pi \end{bmatrix} \tag{A.2}$$

- Lognormal distribution

  Assume the input follows a Lognormal distrbution, with $x \sim \texttt{LN}(b_1, b_2)$ where b_1 is the log mean and b_2 is the log stand deviation. Then the two parameters can be expressed using its mean ad standard deviation as:

$$b_1 = \ln\left(\frac{\mu^2}{\sqrt{\mu^2+\sigma^2}}\right); \quad b_2 = \sqrt{\ln\left(1+\frac{\sigma^2}{\mu^2}\right)} \tag{A.3}$$

  from which, the Jacobian matrix for re-parameterization can be formed as:

$$\mathbb{J} = \begin{bmatrix} \frac{2}{\mu} - \frac{\mu}{\mu^2+\sigma^2} & -\frac{\sigma}{\mu^2+\sigma^2} \\ \frac{1}{b_2}\frac{-\sigma^2}{(\mu^2+\sigma^2)\mu} & \frac{1}{b_2}\frac{-\sigma}{(\mu^2+\sigma^2)} \end{bmatrix} \tag{A.4}$$